

Article

Fabrication of rGO/Fe₃O₄ Magnetic Composite for the Adsorption of Anthraquinone-2-Sulfonate in Water Phase

Shuangyang Zhao ¹, Meixi Li ¹, Jie Ding ^{1,*}, Shanshan Yang ^{1,*}, Yani Zang ¹, Yan Zhao ^{2,3}, Xinlei Gao ^{2,3} and Nanqi Ren ¹

¹ State Key Laboratory of Urban Water Resource and Environment, School of Environment, Harbin Institute of Technology, Harbin 150090, China; zsy88530@163.com (S.Z.); Macey1998@163.com (M.L.); zangyani123@163.com (Y.Z.); rnq@hit.edu.cn (N.R.)

² Harbin Institute of Technology National Engineering Research Center of Water Resources Co., Ltd., Harbin 150090, China; Zhaoyan@126.com (Y.Z.); gaoxinleiuser@126.com (X.G.)

³ Guangdong Yuehai Water Investment Co., Ltd., Shenzhen 518021, China

* Correspondence: dingjie123@hit.edu.cn (J.D.); shanshanyang@hit.edu.cn (S.Y.)

Abstract: In the last few decades, anthraquinone and its derivatives (AQs) have been intensively applied to electrochemical, textile and dye, and photovoltaic industries. This has increased the levels of AQs in the natural environment and threatens human health. To remove AQs from the aqueous phase and recover these multi-functional molecules, a binary magnetic adsorbent, reduced graphene/Fe₃O₄ (rGO/Fe₃O₄), was synthesized via a hydrothermal method. Transmission electron microscopy (TEM), X-ray diffraction (XRD), Fourier transform infrared (FTIR), Raman spectra, and thermogravimetric analysis (TGA) were then used to characterize the samples. The adsorption capacities of rGO/Fe₃O₄ to AQs were investigated by selecting anthraquinone-2-sulfonate (AQ2S) as a model molecule. The adsorption process followed the Langmuir adsorption isotherm and the second-order kinetics. The regeneration of adsorbents and the recycling of AQ2S and solvent were simultaneously achieved by Soxhlet extraction and rotary evaporation. These results confirm the high adsorption efficiency of rGO/Fe₃O₄ for removing AQs from water and provide a promising approach to recover the valuable molecules from the aqueous phase.

Keywords: adsorption; magnetic composite; anthraquinone-2-sulfonate; regeneration



Citation: Zhao, S.; Li, M.; Ding, J.; Yang, S.; Zang, Y.; Zhao, Y.; Gao, X.; Ren, N. Fabrication of rGO/Fe₃O₄ Magnetic Composite for the Adsorption of Anthraquinone-2-Sulfonate in Water Phase. *Water* **2021**, *13*, 2315. <https://doi.org/10.3390/w13172315>

Academic Editor: Chicgoua Noubactep

Received: 19 July 2021

Accepted: 20 August 2021

Published: 24 August 2021

Publisher's Note: MDPI stays neutral with regard to jurisdictional claims in published maps and institutional affiliations.



Copyright: © 2021 by the authors. Licensee MDPI, Basel, Switzerland. This article is an open access article distributed under the terms and conditions of the Creative Commons Attribution (CC BY) license (<https://creativecommons.org/licenses/by/4.0/>).

1. Introduction

Recently, anthraquinone and its derivatives (AQs) have attracted increasing attention because of their excellent electrochemical properties and good visible-light responses [1]. As non-precious metal electrode materials, AQs have been intensively applied to develop environmentally friendly batteries that have high voltage and better energy-storage capacities [2]. They are also used to degrade refractory organic pollutants in advanced electrochemical oxidation processes (EAOPs) [3]. Their conjugated double bonds increase their capacity for light absorption [4]. Furthermore, AQs are effective photosensitizers, and are widely used for solar energy storage, in the textile dyeing processes [5,6], and for the development of biosensors [7]. However, the high solubility of AQs in water limits their applications as they enter the natural environment in dissolution and threaten human health.

To overcome this, continuous efforts have been made to eliminate AQs from aqueous environments. These methods include bacterial degradation, advanced oxidation processes, physical techniques, and electrochemical oxidation [8–10]. Due to their numerous applications and complex synthesis, advanced recycling methods are required to remove AQs without damaging their inherent activity during the cycling process. Adsorption is recognized as an easy, low-cost, and efficient pollutant removal method, which has

been widely used to remove pollutants and capture valuable molecules from water [11,12]. Adsorbents play critical roles in improving the extraction of target pollutants from water.

Graphene, a two-dimensional carbon material, is widely used in material science and technology, due to its distinctive structural, mechanical, and electronic properties [13,14]. Graphene's ultrahigh-specific surface area and high delocalized p-electron system make it a viable option for the removal of organic contaminants, with a strong affinity and high adsorption capacity [15]. Theoretically, AQs with abundant conjugated double bonds can firmly attach to the surface of graphene, which has a specifically developed, π - π stacked, two-dimensional conjugated structure, without a covalent bond [16,17]. Therefore, using graphene as an adsorbent is a suitable solution for the absorption of AQs from water. However, graphene must be centrifuged or filtered after water treatment, to separate and recycle the adsorbent, which is inconvenient and tedious [18]. To overcome these limitations, magnetic materials such as iron oxide nanomaterials have been widely used for the simple removal of dispersive tiny targets using an external magnet [19]. Yao et al. [20] applied a coprecipitating method to generate Fe_3O_4 particles, and then added hydrazine hydrate as a reduction into a graphene oxide and Fe_3O_4 mixed solution to form an rGO/ Fe_3O_4 composite [20]. Although this as-prepared binary material showed a good performance of Congo red (CR) adsorption methylene blue (MB), the use of hydrazine hydrate may be a safety hazard because it is highly corrosive. Liu et al. [18] constructed a GO/ Fe_3O_4 magnetic adsorbent for Cr(VI) removal, via an intricate electrostatic assembling method [18]. Wei et al. [21] provided a solvothermal method to generate Fe_3O_4 particles, and then obtained the GO/ Fe_3O_4 composite by electrostatic interaction [21]. Due to the defect of the π - π conjugate on the GO surface, the as-obtained material is not ideal as an adsorbent for the removal of AQ2S. Therefore, the development of an effective method to produce rGO/ Fe_3O_4 is required.

To fulfill ecological and economic demands, the regeneration and reuse of adsorbents are essential in practical applications, which also reduces the overall cost of the adsorption process. The Soxhlet extraction process is an ideal approach for the regeneration of adsorbents due to very small mass loss, reduced solvent cost, and little damage to the structures of adsorbates and adsorbents [22,23].

In this study, a binary magnetic adsorbent, reduced graphene oxide- Fe_3O_4 (rGO- Fe_3O_4), was constructed by a one-pot hydrothermal method and used to remove organic pollutants from the aqueous phase. A typical AQ, anthraquinone-2-sulfonate (AQ2S), was used as a model pollutant. The as-prepared composite had an excellent adsorption capacity for AQ2S and showed good separation performance from the suspension. Soxhlet extraction was used as the regeneration method, and the extract was concentrated by a rotary evaporator to recover the AQ2S. This combination of Soxhlet extraction and rotary evaporation not only recovered the AQ2S, but also significantly reduced the organic solvent consumption. In addition, a five-cycle experiment was performed to investigate the stability of the adsorbent. The flow chat of the AQ2S adsorption/recovery process is shown in Figure 1.

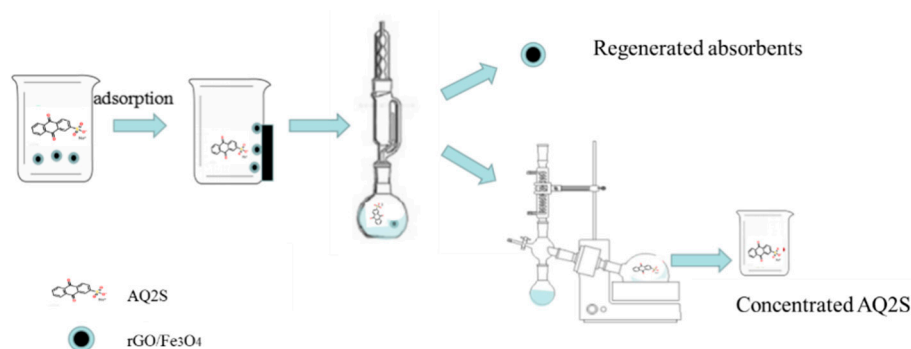


Figure 1. Flow chat of the AQ2S adsorption/recovery process with rGO/ Fe_3O_4 .

2. Material and Methods

2.1. Chemicals and Reagents

Sodium anthraquinone-2-sulfonate was purchased from Shanghai Aladdin Corporation. NaHCO_3 , HCl , NaCl , methanol, and NaOH were given by Tianjin Continental Chemical Reagent Factory (Tianjin, China). Sodium dodecylbenzene sulfonate (SDBS) was supplied by Tianjin Tianli Chemical Reagent Co., Ltd. Graphene oxide (GO) was obtained from Tangshan Jianhua Science Technology Co., Ltd. Ferrous chloride tetrahydrate ($\text{FeCl}_2 \cdot 4\text{H}_2\text{O}$) and Iron chloride hexahydrate ($\text{FeCl}_3 \cdot 6\text{H}_2\text{O}$) were obtained from Tianjin Shuangchuan Chemical Reagent Factory. All the reagents were analytical grade and did not require any further purification. All the experiment was done using deionized (DI) water.

2.2. Synthesis of Fe_3O_4 Nanoparticles

In an alkaline solution, Fe^{2+} and Fe^{3+} were chemically coprecipitated to produce magnetic Fe_3O_4 [24]. $\text{FeCl}_2 \cdot 4\text{H}_2\text{O}$ (0.06 g) and $\text{FeCl}_3 \cdot 6\text{H}_2\text{O}$ (0.12 g) were solubilized in deionized water, and 1 M NaOH solution was used to maintain the pH at 10. After 120 min of stirring at 50°C , the solution was cooled and black precipitates from the solution were then separated with external magnet. Before being dried at 60°C under decreased pressure, the precipitate was washed several times with ethanol and DI water.

2.3. Synthesis of rGO/ Fe_3O_4 Composite

A one-pot hydrothermal approach was employed to make the rGO/ Fe_3O_4 composites, which used sodium dodecylbenzene sulfonate (SDBS) as an anionic surfactant for micelles formation in water [25]. Typically, 25 mg of SDBS was dissolved in 10 mL DI water. The, GO (8.1 mg) and Fe_3O_4 (0.323 g) were introduced to the SDBS solution and ultrasonicated for 40 min. For the hydrothermal process, the suspension was heated to 180°C in a 100 mL Teflon-lined autoclave for 16 h. The solution was permitted to cool down to ambient temperature. The solid was rinsed with deionized water (DI) and ethanol multiple times before being dried in a vacuum oven for 12 h at 60°C .

2.4. Characterization

The structures and morphologies of prepared composites were analyzed through transmission electron microscopy (TEM FEI Tecnai F20, Waltham, MA, USA). A diffractometer of X-ray (X'Pert, Panalytical, Almelo, The Netherlands) was used to acquire sample X-ray diffraction (XRD) patterns using the radiation of $\text{Cu K}\alpha$ in the 2θ range from 10° to 90° . A spectrometer of Raman (inVia-Reflex, Renishaw, Wotton-under-Edge, UK) equipped with a 532 nm laser was used to record the products' Raman spectra. Over the range of $4000\text{--}400\text{ cm}^{-1}$, Fourier transform infrared (FT-IR) spectra were collected on an infrared spectrometer (Nicolet iS50, Thermo Fisher, Waltham, MA, USA) with KBr as a background. Quantachrome Autosorb IQ (Waltham, MA, USA) examined the pore size distribution and specific surface area of photosensitive particles. The chemical states and surface elemental compositions of each specimen were assessed using X-ray photoelectron spectroscopy (XPS, PHI 5300, Perkin Elmer, Waltham, MA, USA) with a source of $\text{Al K}\alpha$ X-ray. The C1s peak at 284.8 eV was implemented to calibrate all binding energies.

2.5. Adsorption Experiments

Batch experiments were used to evaluate SDZ adsorption characteristics and the AQ2S adsorption mechanism on rGO/ Fe_3O_4 . Kinetic experiments were analyzed by adding 10 mg adsorbent to a series of 250 mL AQ2S solutions with $50\text{ mg}\cdot\text{L}^{-1}$. Samples were taken and analyzed after 0.5, 1, 2, 3, and 4 h adsorption, at 288, 298, and 308 K temperature, which represent the average temperatures of wastewater-treatment plants in winter, spring/autumn, and summer, respectively. The vials were transferred to an incubator shaker and shaken at 150 rpm. The adsorbent was separated magnetically from

the suspension and HPLC was used to measure residual AQ2S concentrations. After magnetic separation, the adsorption amounts q_t (mg/g) were calculated by Equation (1):

$$q_t = \frac{(c_0 - c_t)v}{m} \quad (1)$$

where v demonstrates the volume of AQ2S solution (mL), m demonstrates the mass of the adsorbent (mg), and C_0 and C_t imply the concentration ($\text{mg}\cdot\text{L}^{-1}$) at zero time (initial) and concentration ($\text{mg}\cdot\text{L}^{-1}$) at time t , respectively.

Adsorption isotherms were obtained by adding 250 mL AQ2S solutions at different concentrations ($5\text{--}100 \text{ mg}\cdot\text{L}^{-1}$) in 500 mL vials with 10 mg rGO/Fe₃O₄ at three temperatures (288, 298, and 308 K) for 8 h. The samples were taken at 0 and 8 h to measure the AQ2S concentrations. All experiments were performed in duplicate.

2.6. Regeneration

The saturated adsorbent was regenerated via Soxhlet extraction using methanol, ethanol, and acetone as solvents. rGO/Fe₃O₄ (10 mg) was placed in the Soxhlet extractor cartridge and repeatedly refluxed with 100 mL methanol at 70, 80, 90, and 100 °C. After extraction, the adsorbent in the cartridge was removed and rinsed several times with DI water followed by its drying at 60 °C. The extract containing AQ2S was poured into the Rotary Evaporator to recover the concentrated AQ2S and methanol.

3. Results and Discussion

3.1. Characterizations of rGO/Fe₃O₄ Composite

The morphology and structure of the as-prepared rGO/Fe₃O₄ are shown in the TEM image (Figure 2). Figure 2a shows that the GO sheets are single-layered and two-dimensional planar structures, with slight wrinkles on their surface. Figure 2b,c, show that the magnetic Fe₃O₄ particles are dispersed on the edges and the wrinkles of rGO's basal planes at a high density. The void blanks between Fe₃O₄ particles indicate that the presence of rGO successfully prevents the aggregation of Fe₃O₄ particles. The length of the (311) face of Fe₃O₄ is measured and shown in Figure 2c, which is consistent with the XRD result.

FT-IR spectroscopy further characterized carbon species and the functional groups of GO, Fe₃O₄, and rGO/Fe₃O₄ (Figure 3a). The characteristic absorption peak of GO and rGO/Fe₃O₄ was present at 1618 cm^{-1} , ascribed to the C-C stretching vibration on the sp² carbon skeleton [13]. The peaks detected at 1368 and 3433 cm^{-1} associated with the stretching vibration of C-O and -OH, respectively. The peak at 580 cm^{-1} for Fe₃O₄ particles and rGO/Fe₃O₄ is due to Fe-O vibrations [21].

The phase compositions and crystal structures were investigated using XRD techniques (Figure 3b). The presence of distinct characteristic peaks in all samples suggests that the composite has high crystallinity. The primary diffraction peaks for Fe₃O₄ crystals were found at 30.2° , 35.5° , 43.2° , and 62.7° , which correspond to the crystal faces (220), (311), (400), (422), (511), and (440). (JPPDS No. 19-0629). The diffraction angle of GO was found to be 10.7° , which corresponded to the GO plane (001). Compared with GO, no obvious peak was present at 10.7° in the composite XRD pattern, which might be due to the reduction of GO during synthesis.

The spectra of Raman revealed the lattice structure of GO and rGO/Fe₃O₄. As seen in Figure 3c, the GO peaks at 1350 and 1590 cm^{-1} belong to the D and G bands, accordingly, which are slightly blue-shifted when compared to pure GO. The average size of the sp² domains [14] is inversely related to the intensity ratio ID/IG, which fell from 1.12 to 1.06 following Fe₃O₄ addition, indicating that the hydrothermal process reduced the rGO and regained the conjugate structure.

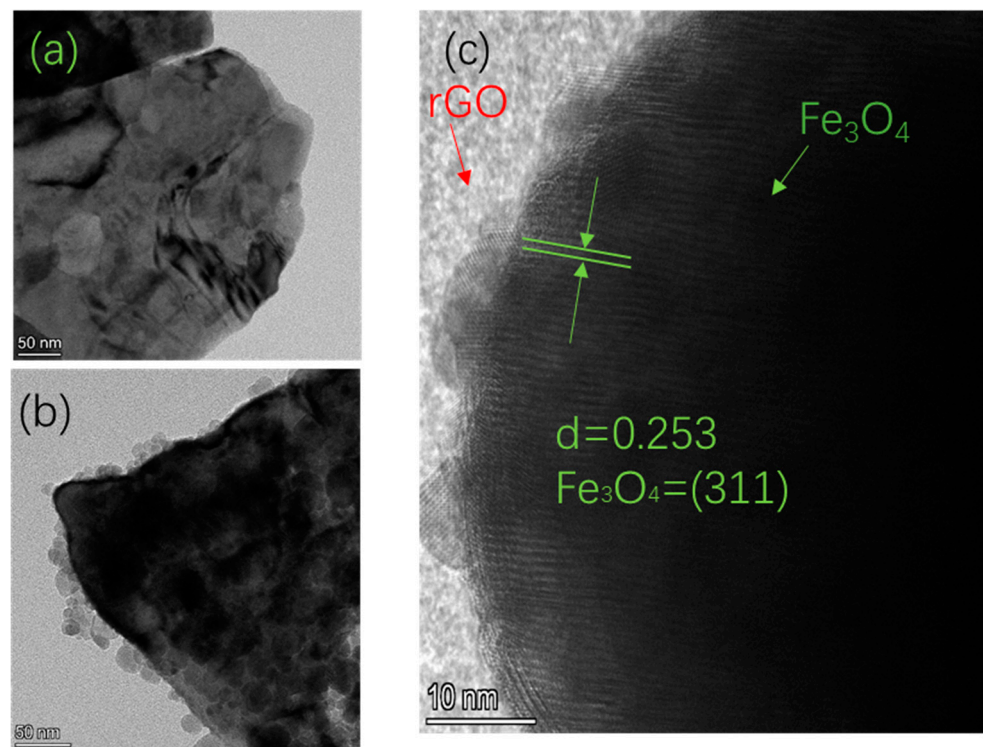


Figure 2. TEM images of (a) GO, (b,c) rGO/Fe₃O₄.

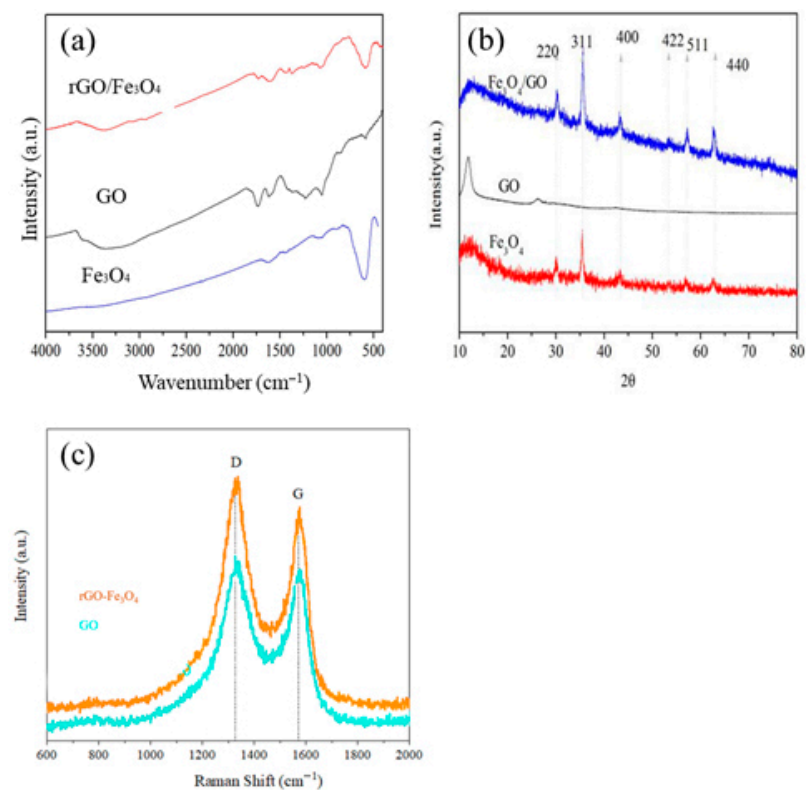


Figure 3. (a) FTIR spectra of GO, Fe₃O₄ and rGO/Fe₃O₄; (b) XRD patterns of GO, Fe₃O₄ and rGO/Fe₃O₄; (c) Raman spectra of GO and rGO/Fe₃O₄.

The chemical states and surface composition of the elements in the rGO/Fe₃O₄ composite are detected using XPS (Figure 4). The as-prepared composite material is made up of O, Fe, and C, as seen in the XPS entire survey spectrum in Figure 4a. C1s and O1s are

responsible for the peaks at 285 and 530 eV, respectively [19]. The characteristic peaks located at 710 eV correspond to Fe 2p. In Figure 4b, peaks at 725.0 and 711.5 eV are allocated to Fe 2p_{1/2} and Fe 2p_{3/2}, accordingly [20].

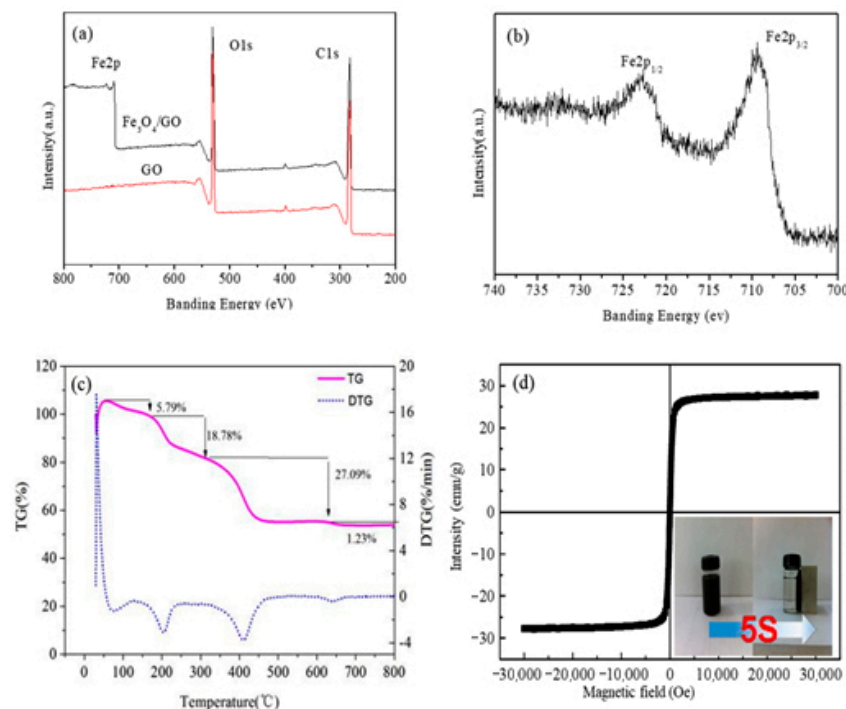


Figure 4. (a) XPS survey spectra of rGO/Fe₃O₄. (b) High-resolution XPS spectra of Fe_{2p}; (c) curves of TG and DTG for rGO/Fe₃O₄ in air atmosphere; (d) Magnetization curves of rGO/Fe₃O₄. Photographic photos of rGO/Fe₃O₄ (left) and its behavior in a magnetic field are shown in the inset (right).

The percentage of each component in rGO/Fe₃O₄ composite was determined by thermogravimetric analysis (TGA), which was carried out at a heating rate of 10 °C min⁻¹ in an air atmosphere. Figure 4c shows the weight loss stages of the composite in air: the first stage occurs at below 150 °C, attributable to water adsorbed on the material's surface evaporating. The elimination of labile oxygen-containing functional groups, including CO and CO₂, and H₂O vapors from the specimen produced through the breakdown of the oxygenated functional groups, causes the second stage of weight loss, which occurs between 150 and 300 °C, to be considerably more evident than the first. Then significant weight loss occurs from 300 to 800 °C, indicating the decomposition of graphene in air. The amount of Fe₃O₄ microspheres in the rGO/Fe₃O₄ composites was estimated to be 47.11% from the residual weight.

The magnetic hysteresis loop of the as-prepared rGO/Fe₃O₄ samples at room temperature is shown in Figure 4d. The composite's saturation magnetization (M_s) value was 22.7 emu/g. Under the influences of external magnetic fields, the dispersed composite in aqueous solution was drawn to the sides of the bottle, demonstrating that the magnetic property of rGO/Fe₃O₄ is sufficient for rapid magnetic separation, which is critical for practical application in water treatment.

Table 1 shows the BET surface areas of the as-obtained materials. According to the BET analysis, the addition of Fe₃O₄ decreased the BET surface areas to 522.134 m²/g, compared with GO (635.21 m²/g). Although the reduction of rGO will increase the surface areas, the decrease caused by inclusion of FeO₄ which increases the adsorption site occupancy.

Table 1. BET computation outcomes for GO and rGO/Fe₃O₄.

Samples	Surface Area (BET) ^a m ² ·g ⁻¹	Pore Volume (P/P ₀ = 0.97) ^b cm ³ ·g ⁻¹	Pore Size (BJH) ^c nm
GO	635.2103	1.402	10.525
rGO/Fe ₃ O ₄	522.1341	1.251	8.633

^a The Burnauer-Emmett-Teller (BET) method was used to measure N₂ adsorption. ^b Determination of total pore volume was carried out at P/P₀ = 0.97. ^c The Barrett-Joyner-Halenda (BJH) method was used to calculate the diameter of the pores based on the desorption data.

3.2. Batch Adsorption Investigations

3.2.1. Adsorption Kinetics

The adsorption of AQ2S on the surface of rGO/Fe₃O₄ is greatly influenced by temperature. The adsorption process of AQ2S is investigated at different temperatures from 288 to 308 K with a 50 mg·L⁻¹ initial concentration of AQ2S, and 10 mg rGO/Fe₃O₄. The adsorption of AQ2S increased as the temperature was raised, showing that the procedure is endothermic (Figure 5a). Because of the fast rate of diffusion of AQ2S on the composite surface at temperatures of 288 and 308 K, all three adsorption processes reached adsorption/desorption equilibrium in 4 h. Furthermore, the AQ2S equilibrium adsorption capacity increases from 288 to 308 K, making it as sensitive as the adsorption rate. The kinetics of the AQ2S adsorption process at different temperatures were studied using the second-order models and pseudo-first. These models are shown in Equations (2) and (3), respectively.

$$\ln(q_e - q_t) = \ln q_e - \frac{k_1}{2.303} t \quad (2)$$

$$\frac{t}{q_t} = \frac{1}{k_2 q_e^2} + \frac{1}{q_e} t \quad (3)$$

where q_t (mg·g⁻¹) and q_e represent the capacities of adsorption at time t (h) and equilibrium, accordingly; v represents the total volume of the suspension (mL); m demonstrates the mass of the adsorbent (mg); k_1 and k_2 represent the pseudo first-order rate constants (h⁻¹) and the rate constant for pseudo second-order adsorption (g·mg⁻¹·h⁻¹), respectively [26].

The calculated results from both pseudo first-order and pseudo second-order models are given in Table 2. The model of pseudo first-order is not fit to represent the adsorption of AQ2S by rGO/Fe₃O₄ based on the correlation coefficient (r^2). Better fit lines at each temperature (Figure 5b) are obtained by plotting t/q_t versus t based on the model of pseudo second-order with a high correlation coefficient > 0.99, which indicates that the adsorption process followed pseudo second-order kinetics. According to a better fit to the model of pseudo second-order, the rate of adsorption is responsible for the distribution of adsorption sites rather than the concentration of adsorbate in the solution.

Table 2. Adsorption kinetic model rate constants for AQ2S adsorption on rGO/Fe₃O₄ at various temperatures.

T/(K)	Pseudo First-Order			Pseudo Second-Order		
	k_1 /(h ⁻¹)	$q_{e,cal}$ /(mg·g ⁻¹)	r_1^2	$k_2 \times 10^{-3}$ /(mg·g ⁻¹ ·h ⁻¹)	$q_{e,cal}$ /(mg·g ⁻¹)	r_2^2
288	0.33	23.11	0.980	1.18	370.37	0.999
298	0.43	18.29	0.984	1.57	384.61	0.994
308	0.38	18.54	0.973	2.14	370.37	0.993

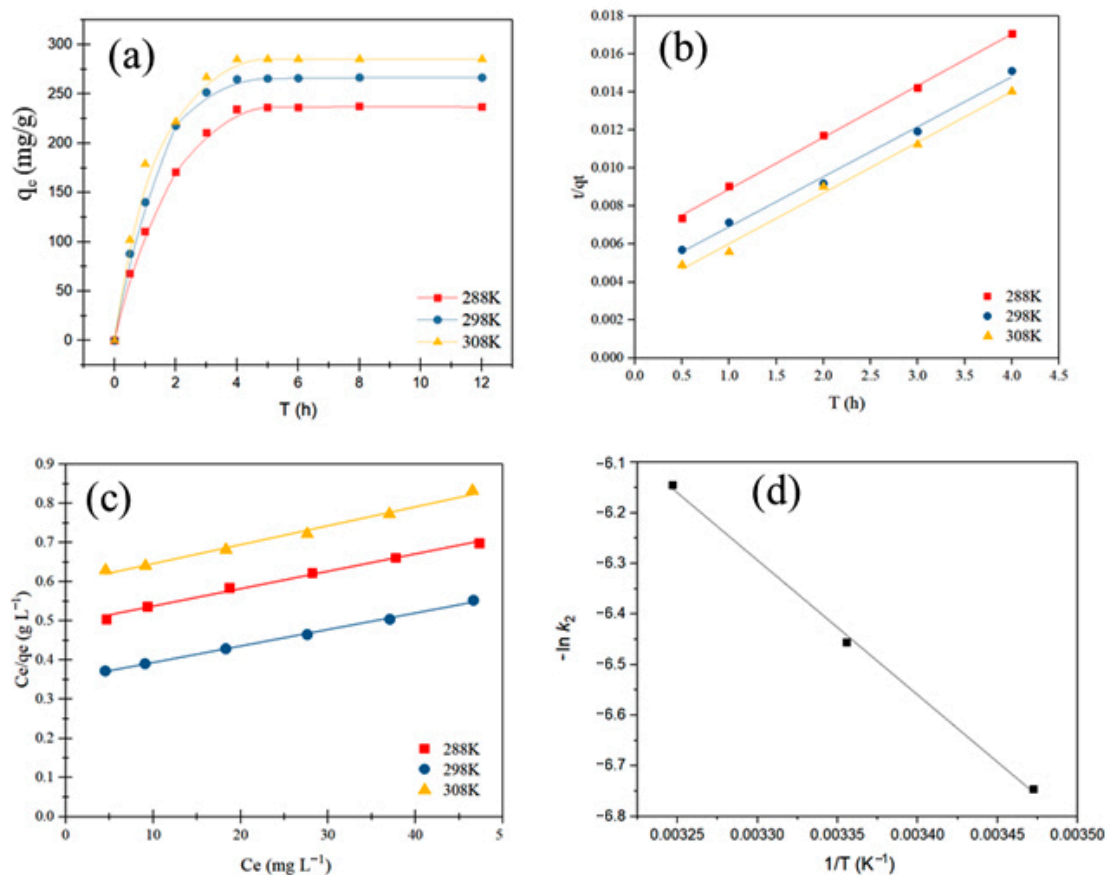


Figure 5. (a) Effect of temperature on the sorption kinetics of AQ2S; (b) Pseudo second-order kinetics of AQ2S at various temperature; (c) Linearized Langmuir isotherms for AQ2S adsorption at different temperature; (d) Determination of the activation energy for AQ2S adsorption.

Due to the better fit of this model, Arrhenius equation (Equation (4)) parameters are reasonable for the determination of the AQ2S adsorption type.

$$k_2 = k \exp(E_a/RT) \quad (4)$$

where k and k_2 are the temperature-independent factor ($\text{g} \cdot \text{mg}^{-1} \cdot \text{h}^{-1}$).

From Figure 5d, the adsorption activation energy ($E_a = 22.13 \text{ kJ} \cdot \text{mol}^{-1}$) calculated from the slope of the plot, reveals that this adsorption process can be considered as physical adsorption ($5\text{--}40 \text{ kJ} \cdot \text{mol}^{-1}$) [27,28].

3.2.2. Adsorption Isotherms

Adsorption isotherms are frequently employed to reveal the adsorbate distribution in the solid and liquid phases at equilibrium. The adsorption of AQ2S by rGO/Fe₃O₄ is explained by employing the Freundlich and Langmuir isotherm models. The linear forms of these two isotherms are listed below:

$$\text{Langmuir : } \frac{C_e}{q} = \frac{C_e}{q_m} + \frac{1}{q_m k_1} \quad (5)$$

$$\text{Freundlich : } \ln q_e = \frac{\ln C_e}{n} + \ln k_f \quad (6)$$

where k_1 and k_f imply the Langmuir constant and Freundlich constant, respectively; q_m illustrates the maximum capacity of adsorption ($\text{mg} \cdot \text{g}^{-1}$); n demonstrates the intensity of adsorption; and C_e is the equilibrium concentration ($\text{mg} \cdot \text{L}^{-1}$) [26].

The linear fit of Langmuir and Freundlich isotherms is shown in Figure 5c, and the calculated parameters are given in Table 3. The Langmuir model better describes the adsorption isotherm of AQ2S due to greater correlation coefficient values ($r^2 > 0.99$). As a result, the adsorption is monolayer adsorption, with a finite number of adsorption sites on the rGO/Fe₃O₄ surface. Once all the sites are occupied by AQ2S, the surface of the adsorbent reaches saturation point [27].

Table 3. Correlation coefficients and parameters of AQ2S adsorption by the Langmuir and Freundlich model.

Model	Parameters	Temperatures (K)		
		288	298	308
Langmuir	$k_L/(L \cdot mg^{-1})$	0.0089	0.0119	0.0080
	$Q_m/(mg \cdot g^{-1})$	227.27	238.10	208.33
	R^2	0.992	0.998	0.990
Freundlich	$K_f/(mg \cdot g^{-1})$	6.91	7.28	14.36
	n	1.23	1.29	7.28
	R^2	0.979	0.983	0.967

3.2.3. Thermodynamic Studies

Thermodynamics analyses are widely used to determine energy changes during the adsorption process, in a wide range of temperatures. Thermodynamic parameters including enthalpy (H°), Gibbs free energy (G°), and entropy (S°) were estimated by utilizing Equations (7) and (8) to examine the effects of temperature on the adsorption of AQ2S by rGO/Fe₃O₄:

$$\ln k_d = \frac{\Delta S^\circ}{R} - \frac{\Delta H^\circ}{RT} \quad (7)$$

$$\Delta G^\circ = \Delta H^\circ - T\Delta S^\circ \quad (8)$$

The calculated results are shown in Table 4. The adsorption of AQ2S on the surface of rGO/Fe₃O₄ is irreversible and endothermic, as indicated by the positive ΔS° and ΔH° values. Furthermore, the negative standard Gibbs free energy ΔG° values at different temperatures indicate that the degree of spontaneity of the reaction and the spontaneous adsorption increase as temperature rise [29].

Table 4. Thermodynamic parameters at various temperatures.

T (K)	ΔG° (KJ·mol ⁻¹)	ΔS (KJ·mol ⁻¹)	ΔH° (KJ·mol ⁻¹)
288	−4.2152		
298	−4.6784	0.046	9.123
308	−5.1415		

3.3. Regeneration of Adsorbent and AQ2S Recovery

To improve the regeneration performance, different parameters such as the effect of solvent, temperature, and regeneration time were optimized. Ethanol showed the best desorption of AQ2S in a shorter time (90 min) and restored approximately 98% adsorption capacity of rGO/Fe₃O₄. The regeneration performance remains constant after 90 min extraction, demonstrating 90 min as the optimum time for the regeneration of rGO/Fe₃O₄. Although the regeneration rate can reach nearly 99% at 90 and 100 °C considering the energy cost, 80 °C is a suitable choice, with a 98% regeneration rate. Therefore, the regeneration of composite with methanol for 90 min at 80 °C results in optimum performance.

Under the optimum conditions, five consecutive adsorption/regeneration cycles were conducted to measure the adsorbent's reproducibility and stability. The result is shown in

Figure 6a which reveals that the rGO/Fe₃O₄ composite maintains its adsorption capacity at 85.7% after five cycles, indicating good stability of this composite. The recovery of AQ2S and methanol was achieved by the rotary evaporation process under negative pressure. Figure 6b shows that, with the increasing index of the adsorption/regeneration cycles, the recovery rate of AQ2S decreased from 92 to 81%, which may be attributed to the mass loss of adsorbent during transferring.

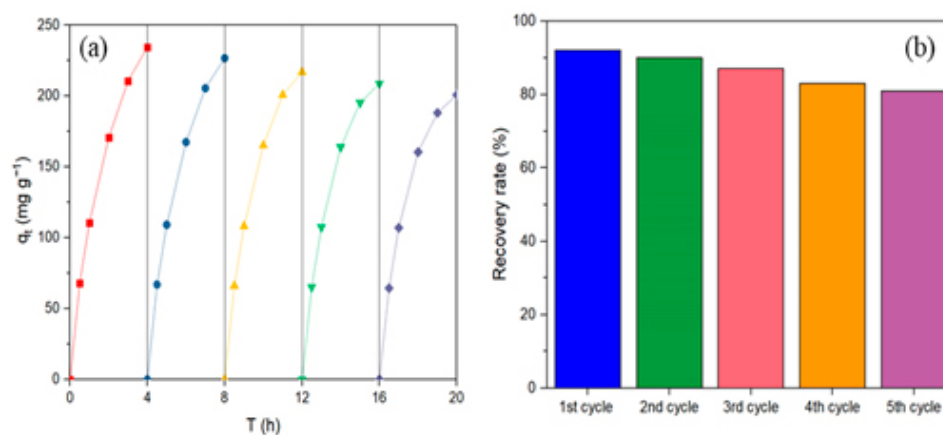


Figure 6. Adsorption capacity (a) and AQ2S recovery rate (b) variation over the adsorption/regeneration cycle.

4. Conclusions

In this study, a binary magnetic rGO/Fe₃O₄ adsorbent was synthesized by the hydrothermal method for AQ2S removal from the water. The as-synthesized composite was characterized by TEM, FTIR, XRD, XPS, Raman spectra, and TGA. The composite displayed good magnetism and high reusability. The adsorption capacities of the magnetic adsorbent were demonstrated by kinetics and equilibrium models. The adsorption of AQ2S by rGO/Fe₃O₄ was better fitted to the Langmuir isotherm model and described more precisely by a pseudo second-order kinetic model. According to thermodynamic studies, the adsorption reaction was found to be spontaneous and endothermic. The spontaneity of the adsorption procedure increased with the rising temperatures. Therefore, the adsorption of AQ2S on rGO/Fe₃O₄ could be regarded as an endothermic physical adsorption process dominated by π - π stacking. This corresponds to previous studies; Yu et al. [30] calculated the binding energy of Aqs on monolayer graphene via DFT study and confirmed that van der Waals dispersion contributed to >80% of the total attractive interaction for this adsorption process. Through the combination of Soxhlet extraction and rotary evaporation, saturated adsorbents maintained over 90% of their original adsorption capacity for AQ2S after five cycles. The used solvent and AQ2S were also recycled for future use.

Author Contributions: Conceptualization, Y.Z. (Yani Zang) and M.L.; methodology, S.Z.; software, M.L.; validation, S.Y., J.D. and N.R.; formal analysis, S.Z.; investigation, S.Z.; resources, J.D.; data curation, M.L.; writing—original draft preparation, S.Z.; writing—review and editing, S.Y.; visualization, X.G.; supervision, N.R.; project administration, J.D.; funding acquisition, Y.Z. (Yan Zhao). All authors have read and agreed to the published version of the manuscript.

Funding: This research was funded by the National Key Research and Development Program of China (2019YFD1100204); the National Nature Science Foundation of China (No. 51778175); the Research and Application of Treatment Technology for High Concentration and Refractory Wastewater (Printing and Dyeing, Pharmaceutical, Chemical) GJSZ2021030907-YF.

Institutional Review Board Statement: Validation.

Informed Consent Statement: Informed consent was obtained from all subjects involved in the study.

Conflicts of Interest: The authors declare no conflict of interest.

References

1. Son, E.J.; Kim, J.H.; Kim, K.; Park, C.B. Quinone and its derivatives for energy harvesting and storage materials. *J. Mater. Chem. A* **2016**, *4*, 11179–11202. [[CrossRef](#)]
2. Yuan, G.; Zhang, G.; Chen, J.; Fu, L.; Xu, L.; Yang, F. The electrochemical activities of anthraquinone monosulfonate adsorbed on the basal plane of reduced graphene oxide by π - π stacking interaction. *J. Solid State Electrochem.* **2013**, *17*, 2711–2719. [[CrossRef](#)]
3. Zhou, Y.; Zhang, G.; Chen, J.; Yuan, G.; Xu, L.; Liu, L.; Yang, F. A facile two-step electroreductive synthesis of anthraquinone/graphene nanocomposites as efficient electrocatalyst for O₂ reduction in neutral medium. *Electrochem. Commun.* **2012**, *22*, 69–72. [[CrossRef](#)]
4. Scharf, H.-D.; Leismann, H.; Ressler, I.; Schleker, W.-G.; Weitz, R.; Fleischhauer, J. Criteria for the Efficiency, Stability, and Capacity of Abiotic Photochemical Solar Energy Storage Systems. *Angew. Chem. Int. Ed.* **1979**, *18*, 652–662. [[CrossRef](#)]
5. Saquib, M.; Muneer, M. Semiconductor mediated photocatalysed degradation of an anthraquinone dye, Remazol Brilliant Blue R under sunlight and artificial light source. *Dye. Pigment.* **2002**, *53*, 237–249. [[CrossRef](#)]
6. McDermott, M.; Kneten, K.; McCreery, R. Anthraquinonedisulfonate adsorption, electron-transfer kinetics, and capacitance on ordered graphite electrodes: The important role of surface defects. *J. Phys. Chem.* **1992**, *96*, 3124–3130. [[CrossRef](#)]
7. Jamaluddin, R.Z.A.R.; Heng, L.Y.; Tan, L.L.; Chong, K.F. A Biosensor for Genetic Modified Soybean DNA Determination via Adsorption of Anthraquinone-2-sulphonic Acid in Reduced Graphene Oxide. *Electroanaly* **2017**, *30*, 250–258. [[CrossRef](#)]
8. Zhao, J.; Wu, T.; Wu, K.; Oikawa, K. Photoassisted Degradation of Dye Pollutants. 3. Degradation of the Cationic Dye Rhodamine B in Aqueous Anionic Surfactant/TiO₂ Dispersions under Visible Light Irradiation: Evidence for the Need of Substrate Adsorption on TiO₂ Particles. *Environ. Sci. Technol.* **1998**, *32*, 2394–2400. [[CrossRef](#)]
9. Banat, I.; Nigam, P.; Singh, D.; Marchant, R. Microbial decolorization of textile-dyecontaining effluents: A review. *Bioresour. Technol.* **1996**, *58*, 217–227. [[CrossRef](#)]
10. Kaushik, P.; Malik, A. Fungal dye decolourization: Recent advances and future potential. *Environ. Int.* **2009**, *35*, 127–141. [[CrossRef](#)]
11. Li, J.; Zhang, K.; Zhang, H. Adsorption of antibiotics on microplastics. *Environ. Pollut.* **2018**, *237*, 460–467. [[CrossRef](#)]
12. Silva, A.H.D.; Miranda, E.A. Adsorption/Desorption of Organic Acids onto Different Adsorbents for Their Recovery from Fermentation Broths. *J. Chem. Eng. Data* **2013**, *58*, 1454–1463. [[CrossRef](#)]
13. Stankovich, S.; Dikin, D.A.; Piner, R.D.; Kohlhaas, K.A.; Kleinhammes, A.; Jia, Y.; Wu, Y.; Nguyen, S.; Ruoff, R.S. Synthesis of graphene-based nanosheets via chemical reduction of exfoliated graphite oxide. *Carbon* **2007**, *45*, 1558–1565. [[CrossRef](#)]
14. Gan, Z.; Wu, X.; Meng, M.; Zhu, X.; Yang, L.; Chu, P.K. Photothermal Contribution to Enhanced Photocatalytic Performance of Graphene-Based Nanocomposites. *ACS Nano* **2014**, *8*, 9304–9310. [[CrossRef](#)]
15. Tang, Y.; Guo, H.; Xiao, L.; Yu, S.; Gao, N.; Wang, Y. Synthesis of reduced graphene oxide/magnetite composites and investigation of their adsorption performance of fluoroquinolone antibiotics. *Colloids Surf. A Physicochem. Eng. Asp.* **2013**, *424*, 74–80. [[CrossRef](#)]
16. Sertkol, S.B.; Esat, B.; Momchilov, A.A. An anthraquinone-functionalized reduced graphene oxide as electrode material for rechargeable batteries. *Carbon* **2017**, *116*, 154–166. [[CrossRef](#)]
17. Novoselov, K.S.; Geim, A.K.; Morozov, S.V.; Jiang, D.; Zhang, Y.; Dubonos, S.V.; Grigorieva, I.V.; Firsov, A.A. Electric Field Effect in Atomically Thin Carbon Films. *Science* **2004**, *306*, 666–669. [[CrossRef](#)]
18. Liu, M.; Wen, T.; Wu, X.; Chen, C.; Hu, J.; Li, J.; Wang, X. Synthesis of porous Fe₃O₄ hollow microspheres/graphene oxide composite for Cr(vi) removal. *Dalton Trans.* **2013**, *42*, 14710–14717. [[CrossRef](#)] [[PubMed](#)]
19. Kong, L.; Lu, X.; Bian, X.; Zhang, W.; Wang, C. Constructing Carbon-Coated Fe₃O₄ Microspheres as Antacid and Magnetic Support for Palladium Nanoparticles for Catalytic Applications. *ACS Appl. Mater. Interfaces* **2011**, *3*, 35–42. [[CrossRef](#)] [[PubMed](#)]
20. Yao, Y.; Miao, S.; Liu, S.; Ma, L.P.; Sun, P.H.; Wang, S. Synthesis, characterization, and adsorption properties of magnetic Fe₃O₄@graphene nanocomposite. *Chem. Eng. J.* **2012**, *184*, 326–332. [[CrossRef](#)]
21. Wei, H.; Yang, W.; Xi, Q.; Chen, X. Preparation of Fe₃O₄@graphene oxide core-shell magnetic particles for use in protein adsorption. *Mater. Lett.* **2012**, *82*, 224–226. [[CrossRef](#)]
22. Steven, B.; Carol, B.; Esther, M.; David, J.M. Comparisons of Soxhlet extraction, pressurized liquid extraction, supercritical fluid extraction and subcritical water extraction for environmental solids: Recovery, selectivity and effects on sample matrix. *J. Chromatogr. A* **2000**, *892*, 421–433.
23. Castro, L.D.; Priego, C.F. Soxhlet extraction: Past and present panacea. *J. Chromatogr. A* **2010**, *1217*, 2383–2389. [[CrossRef](#)]
24. Jiang, R.; Wu, D.; Lu, G.; Yan, Z.; Liu, J.; Zhou, R.; Nkoom, M. Fabrication of Fe₃O₄ quantum dots modified BiOCl/BiVO₄ p-n heterojunction to enhance photocatalytic activity for removing broad-spectrum antibiotics under visible light. *J. Taiwan Inst. Chem. Eng.* **2019**, *96*, 681–690. [[CrossRef](#)]
25. Malathi, A.; Madhavan, J.; Ashokkumar, M.; Arunachalam, P. A review on BiVO₄ photocatalyst: Activity enhancement methods for solar photocatalytic applications. *Appl. Catal. A Gen.* **2018**, *555*, 47–74.
26. Barkat, M.; Nibou, D.; Chegrouche, S.; Mellah, A. Kinetics and thermodynamics studies of chromium(VI) ions adsorption onto activated carbon from aqueous solutions. *Chem. Eng. Process. Process. Intensif.* **2009**, *48*, 38–47. [[CrossRef](#)]
27. Tan, G.; Dan, X. Adsorption of cadmium ion from aqueous solution by ground wheat stems. *J. Hazard. Mater.* **2009**, *164*, 1359–1363. [[CrossRef](#)]
28. Ji, L.; Chen, W.; Duan, L.; Zhu, D. Mechanisms for strong adsorption of tetracycline to carbon nanotubes: A comparative study using activated carbon and graphite as adsorbents. *Environ. Sci. Technol.* **2009**, *43*, 2322–2327. [[CrossRef](#)] [[PubMed](#)]

-
29. Boparai, H.K.; Joseph, M.; O'Carroll, D.M. Kinetics and thermodynamics of cadmium ion removal by adsorption onto nano zerovalent iron particles. *J. Hazard. Mater.* **2011**, *186*, 458–465. [[CrossRef](#)] [[PubMed](#)]
 30. Yu, Y.-X. A dispersion-corrected DFT study on adsorption of battery active materials anthraquinone and its derivatives on monolayer graphene and h-BN. *J. Mater. Chem. A* **2014**, *2*, 8910–8917. [[CrossRef](#)]